Dithiapyrannylidenes as Efficient Hole Collection Interfacial Layers in Organic Solar Cells

Stéphane Berny,[†,‡] Ludovic Tortech,[†,‡] Michelle Véber,[§] and Denis Fichou*[,†,‡]

CEA-Saclay, Organic Nanostructures and Semiconductors Group, SPCSI/IRAMIS, F-91191 Gif-sur-Yvette, France, UPMC, IPCM, UMR CNRS 7201, 4 place Jussieu, 75005 Paris, France, and Université Paris-Sud 11, UMR CNRS 8502, F-91405 Orsay, France

ABSTRACT One inherent limitation to the efficiency of photovoltaic solar cells based on polymer/fullerene bulk heterojunctions (BHJs) is the accumulation of positive charges at the anodic interface. The unsymmetrical charge collection of holes and electrons dramatically decreases the short-circuit current. Interfacial layers (IFLs) such as poly(3,4-ethylenedioxythiophene):poly(4-styrenesulfonate) have no effect on the unbalanced electron/hole transport across the BHJ. We report here on the use of dithiapyrannylidenes (DITPY), a new class of planar quinoid compounds, as efficient hole-transporting/electron-blocking layers in organic solar cells based on poly(3-hexylthiophene)/[6,6]-phenyl-C_{61}-butyric acid methyl ester (P3HT:PCBM) BHJs. Inserting a 15-nm-thick IFL of 4,4′-bis(diphenyl-2,6-thiapyrannylidene) (DITPY-Ph_4) between the indium−tin oxide electrode and the P3HT:PCBM BHJ prevents detrimental space-charge effects and favors recombination-limited currents. Current-sensing atomic force microscopy reveals a drastic increase of the hole-carrying pathways in DITPY-Ph_4 compared to PEDOT:PSS. In ambient conditions, photovoltaic cells using DITPY-Ph_4 exhibit an 8% increase in the current density, although the conversion efficiency remains slightly lower compared to PEDOT:PSS-based devices. Finally, we present a detailed analysis of the photocurrent generation, showing that DITPY-Ph_4 IFLs induce a transition from unproductive space-charge-limited currents to recombination-limited currents.

KEYWORDS: organic solar cells • photovoltaic devices • interfacial layers • current-sensing atomic force microscopy • space-charge-limited current

1. INTRODUCTION

Organic solar cells (OSCs) have gained particular attention during the past few years and appear to be a rational outlook for large-scale commercialization of low-cost energy (1−5). One of the most efficient systems consists of a bulk heterojunction (BHJ) based on poly(3-hexylthiophene) (P3HT) and [6,6]-phenyl-C_{61}-butyric acid methyl ester (PCBM) (6−8). Recently, a power conversion efficiency (PCE) of 7.4% has been reported on a PTB7/PCBM BHJ (3). Besides design of the active materials, a strategy aiming at improving the OSC performances consists of tailoring the organic/inorganic interfaces (8−12). Conducting polymer-based interfacial layers (IFLs) are commonly used to modify indium−tin oxide (ITO) because they ensure an electrical ohmic contact and minimize the roughness of the oxide in electronic devices (13, 14). Poly(3,4-ethylenedioxythiophene):poly(4-styrenesulfonate) (PEDOT:PSS) is routinely used as an IFL in OSCs, increasing the open-circuit voltages (V_{oc}) and improving the hole collection. However, PEDOT:PSS also possesses several counterproductive properties, such as ITO corrosion (8, 12). In addition, these thin films develop severe structural and electrical inhomogeneities, leading to an out-of-plane conductivity as low as 10^{-3} S · cm^{-1} and weak electron-blocking (EBL) properties (10, 15, 16). The addition of secondary dopants (15), variations in the pH (13), solvents (14), and water contents (17), as well as highly polymerized PEDOT (15) offer attractive features but do not avoid crosstalk across the material (16, 18, 19) and a weak patterning with ITO (8, 12, 15), which lowers OSC efficiencies.

A variety of other organic materials have been tested in order to tune the hole injection at the ITO interface. For example, grafting dipolar self-assembled monolayers such as 4-nitrophenylthiolate (20), halogenated propylsilanes (21), or fluorinated thiols (22) onto ITO strongly enhances charge injection/collection in organic light-emitting devices (OLEDs) and OSCs. The IFL can also play a major role in the growth mode of the active layer (11, 21), increase the hole sensitivity of the electrode defined by its current channel distribution (19, 23), and correct the energy level misalignements (8, 12, 20, 21, 24, 25). For example, Choulis et al. reported that inserting poly(9,9-dioctylfluorene-*co*-*N*-(4-butylphenyl)-diphenylamine) between a PEDOT:PSS IFL and a polyfluorene-based emitting layer drastically improves the hole-injection properties through the anode by the creation of a stepped electronic profile (26). Marks et al. have recently transferred the principle of hole-transporting (HTL)/EBL IFLs developed in OLEDs to the technology of OSCs (8, 10). They reported that inserting an IFL composed of a blend of two

* To whom correspondence should be addressed. E-mail: denis.fichou@cea.fr.
Received for review June 25, 2010 and accepted October 11, 2010
† CEA-Saclay, Organic Nanostructures and Semiconductors Group, SPCSI/IRAMIS.
‡ UPMC, IPCM, UMR CNRS 7201.
§ Université Paris-Sud 11, UMR CNRS 8502.
DOI: 10.1021/am1005546

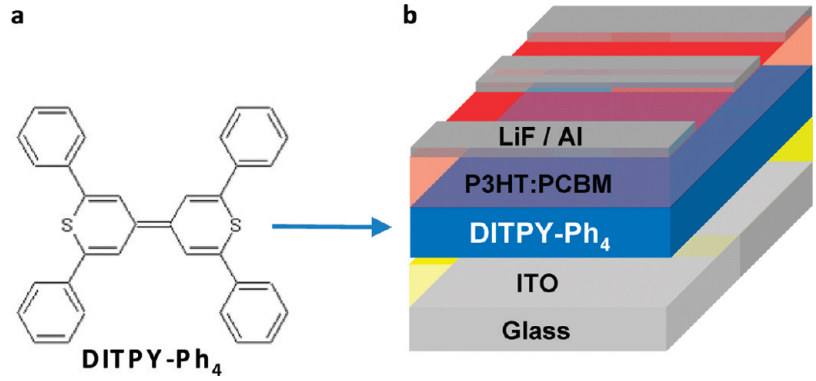

FIGURE 1. (a) Molecular structure of DITPY-Ph$_4$. (b) Typical device architecture of a P3HT:PCBM solar cell using a single DITPY-Ph$_4$ IFL.

p-type semiconductors between ITO and a poly[2-methoxy-5-(3,7-dimethyloctyloxy)-1,4-phenylene-vinylene] (MDMO−PPV):PCBM BHJ leads to a substantial increase in V_{oc}, PCE, and the thermal stability compared to solar cells without IFLs (8, 10, 12). In spite of these fruitful advances, little attention has been devoted to the impact of IFLs on the limitations inherent to polymer/fullerene solar cells as they have been identified by Blom et al. (27−29). Because of their unbalanced charge transport between electrons and holes, polymer/fullerene-based OSCs are generally characterized by an unsymmetrical charge collection, dictated by the accumulation region of holes near the anode.

We have recently synthesized a series of 2,6-dithiapyrannylidenes (DITPY; Figure 1a) in which two thiapyrannylidene heterocycles are linked together by an exocyclic C═C double bond in a para position relative to the S-atom derivatives. The quinoid structure of the DITPY core is reminiscent of tetrathiafulvalene (TTF), a well-known family of π donors with potential applications in molecular electronics (30−32). However, in sharp contrast with TTF and its analogues, whose properties have been extensively studied, DITPY derivatives remain almost unexplored today. DITPY compounds are isoelectronic of TTF and also behave as strong π donors and excellent precursors of 1D organic conductors when substituted by phenyl groups (33, 34). 4,4′-Bis(diphenyl-2,6-thiapyrannylidene) (DITPY-Ph$_4$) is obtained by attaching four phenyl groups in the α positions on the DITPY core (35). In the solid state, DITPY-Ph$_4$ possesses a quasi-planar conformation with phenyl rings tilted by 12° relative to the DITPY core. Finally, DITPY-Ph$_4$ has a low oxidation potential (E_{ox} = 0.3 V) compared to other pyrannylidene derivatives (35). Therefore, the highest occupied molecular orbital (HOMO) energy level of DITPY-Ph$_4$ (−4.8 eV) almost aligns with that of P3HT (−5.0 eV) to create an efficient hole transfer from the active layer (8, 10, 12).

We show here that inserting a DITPY-Ph$_4$ (15 nm) IFL between ITO and the P3HT:PCBM active layer allows one to optimize hole extraction (Figure 1b). Our aim is to describe how such behavior is achieved. We combine IFL investigations at the nanoscale by current-sensing atomic force microscopy (CS-AFM) together with photocurrent measurements in photovoltaic (PV) devices in order to access charge-generation and transport mechanisms. CS-AFM reveals a drastic 360% increase of the hole-carrying pathways in DITPY-Ph$_4$ compared to PEDOT:PSS. In order to describe the driving force of hole collection by DITPY-Ph$_4$ layers, we study them as independent HTL/EBL and as part of a double IFL associated with PEDOT:PSS. The insertion of a DITPY-Ph$_4$ IFL systematically reduces unproductive space-charge effects and leads to a ∼23% increase in PCE compared to equivalent PEDOT:PSS-based OSCs without DITPY-Ph$_4$.

2. EXPERIMENTAL SECTION

Synthesis. The synthesis of DITPY-Ph$_4$ has been described previously (34). In brief, the procedure consists of Friedel−Craft acylation of the side group on glutaryl chloride followed by oxidation with P_2S_5 to obtain a cyclic thiopyrilium salt. The latter compound is then reduced with zinc powder to reach the final product DITPY-Ph$_4$. The detailed experimental procedure is provided in the Supporting Information (SI).

Photoemission Spectroscopy. The photoemission spectra are collected with a hemispherical energy analyzer (AR65, Omicron). The photon energy is 21.2 eV. The secondary electron cutoff is measured with a −6.00 V sample bias.

Tapping-Mode AFM. AFM measurements are all performed at ambient atmosphere using a commercial microscope (multimode equipped with a CS-AFM module and a PicoSPM-LE controller, Molecular Imaging, Agilent Technology).

CS-AFM. For CS-AFM measurements, the AFM is set in a contact mode using $PtIr_5$-coated tips. The tip radius is ∼25 nm, and the contact area is estimated at ∼10 nm, using the Hertz model. ITO forms the back contact. The electrical mapping presented in Figure 3 is reproduced on several areas (>20) of DITPY-Ph$_4$ and PEDOT:PSS thin films. Each current−electric field (I−E) characteristic presented in Figure 4 is the average of more than 40 curves recorded at different locations.

Organic Photovoltaics (OPV) Device Fabrication. The ITO-coated glass substrates (Sigma-Aldrich; 2.5 × 2.5 cm^2; R = 75 ± 5 Ω · cm^{-2}) are patterned, cleaned, and exposed to UV ozone according to a classical procedure. PEDOT:PSS (Sigma-Aldrich; water solution 1.3% in weight) layers are prepared on ITO by spin-coating and further annealed at 120 °C under argon for 30 min. The DITPY-Ph$_4$ thin films (∼15 nm) are deposited, by vacuum-thermal evaporation, with the thickness being monitored by a quartz microbalance. Depending on the device architecture, the blend of regioregular P3HT (Sigma-Aldrich; purity >98.5%) and PCBM (Sigma-Aldrich; purity 99.5%) solubilized in chlorobenzene is deposited on either bare ITO, ITO/PEDOT:PSS, ITO/DITPY-Ph$_4$, or ITO/DITPY-Ph$_4$/PEDOT:PSS. The spin-coating conditions as well as the ratio of the two components (1:0.8) and the annealing conditions (110 °C under argon and 10 min) are adjusted to yield optimized 110-nm-thick films. The devices are completed by successive thermal evaporation of LiF (7 Å) and Al (80 nm), leading to individual PV cells having

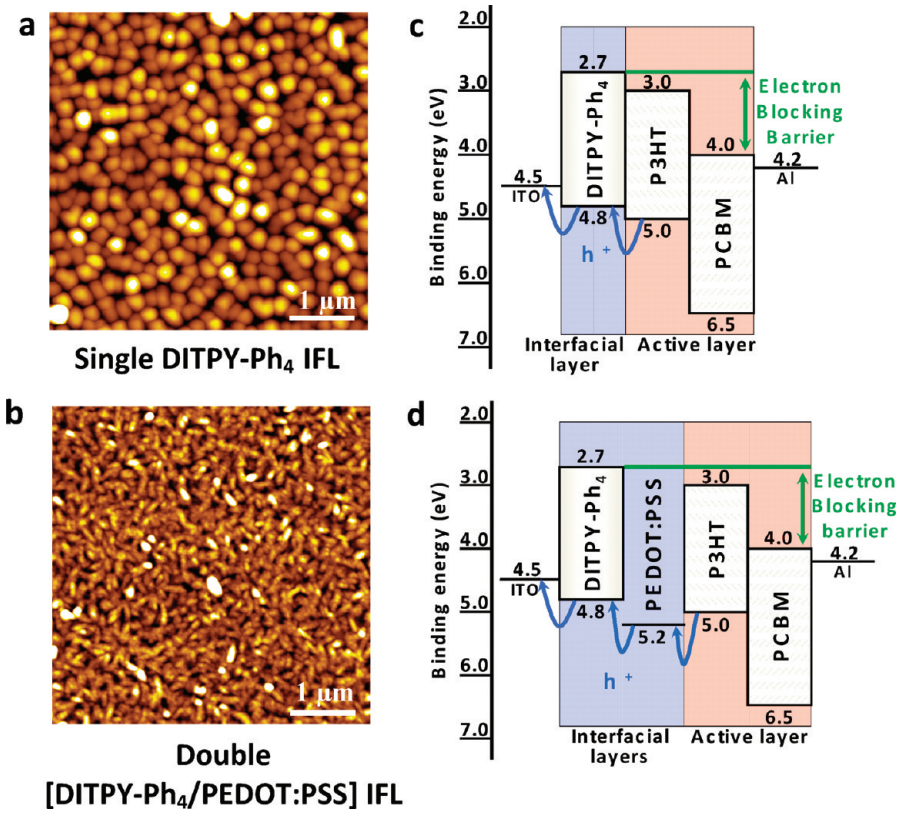

FIGURE 2. Tapping-mode AFM topography images (5 × 5 μm^2) of (a) a single DITPY-Ph$_4$ IFL and (b) a double IFL [DITPY-Ph$_4$/PEDOT:PSS]. Adding the 5-nm-thick PEDOT:PSS layer on top of DITPY-Ph$_4$ strongly changes the topography and the roughness: rms = 5.5 nm for the single IFL and rms = 3.2 nm for the double IFL. Energy diagrams associated with the configurations of both types of devices: (d) with a single DITPY-Ph$_4$ IFL; (e) with a double DITPY-Ph$_4$/PEDOT:PSS IFL.

active areas of 0.15 cm^2. Except vacuum deposition of LiF and Al, all devices are fabricated under ambient conditions.

OPV Device Testing. Current−voltage characteristics are recorded in the dark and under air mass 1.5 global (AM 1.5G) illumination using a Keithley 2602 source meter. The white light supplier is a xenon lamp (Oriel Instruments, 300 W) coupled with a AM 1.5G filter at 75 mW · cm^{-2}. A set of neutral filters is used for light-intensity measurements. All tests are performed in air.

3. RESULTS AND DISCUSSION

At slow evaporation rates (below 0.1 Å · s^{-1}), the DITPY-Ph$_4$ films are polycrystalline with a uniform surface made of monodisperse grains, as revealed by AFM (Figure 2a). Secondary electron spectra exhibit an onset of secondary electrons 0.3 eV higher than that of bare ITO ($\phi_f = -4.5$ eV). As a consequence, the HOMO level of DITPY-Ph$_4$ IFL is located at −4.8 eV. This energy level is close enough to that of P3HT in order to ensure an efficient hole transfer from the P3HT phase to the DITPY-Ph$_4$ IFL, as suggested by recent results obtained on polymer/fullerene solar cells (8, 10−12). Besides the energy of the positive integer, the charge-transfer state of the DITPY-Ph$_4$ film is measured at $E_{ICT}^{+} = -4.29$ eV. Considering pure spectroscopic considerations (36), this is conveniently higher than that of P3HT $E_{ICT}^{+} = -4.00$ eV to extract holes from P3HT. We also note that the HOMO level of DITPY-Ph$_4$ IFLs should also form an electrical ohmic contact with ITO, which strongly favors the hole extraction to the external circuit of solar cells. Finally, the lowest unoccupied molecular orbital (LUMO) level of DITPY-Ph$_4$ IFLs is measured 0.3 eV higher than that of P3HT by UV−visible spectrometry. This additional energy barrier may be responsible for the EBL properties (Figure 2).

3.1. Characterization by CS-AFM.

CS-AFM measurements associate the mapping of current-carrying pathways of organic thin films with a topography image. They also allow determination of the charge-carrier mobility by single-point spectroscopy measurements. The electron injection efficiency into the DITPY-Ph$_4$ layer can be neglected because both work functions of ITO ($\phi_f = -4.5$ eV) and of $PtIr_5$ ($\phi_f = -5.6$ eV) tips are high. As a consequence, the current is unipolar, corresponding to an out-of-plane transport of holes, similar to the one implied in macroscopic OSCs.

3.1.1. Electrical Mapping of DITPY-Ph$_4$ and PEDOT:PSS IFLs. Current-Carrying Pathways of a DITPY-Ph$_4$ IFL. The CS-AFM current image performed on the DITPY-Ph$_4$ IFL at −600 mV highlights large electrical contrasts (Figure 3b). These bright regions are distributed on the entire organic surface and correspond to hole-carrying pathways of the individual DITPY-Ph$_4$ grains, as confirmed by the topography image detected simultaneously (Figure 3a). The comparison between current and topography images also reveals that electrical channels preferentially appear at the periphery of the grains, that is at low thicknesses. This indicates a thickness-dependence of the current intensity, which is attributed to a specific hole-transport mechanism in the DITPY-Ph$_4$ thin film, as described below.

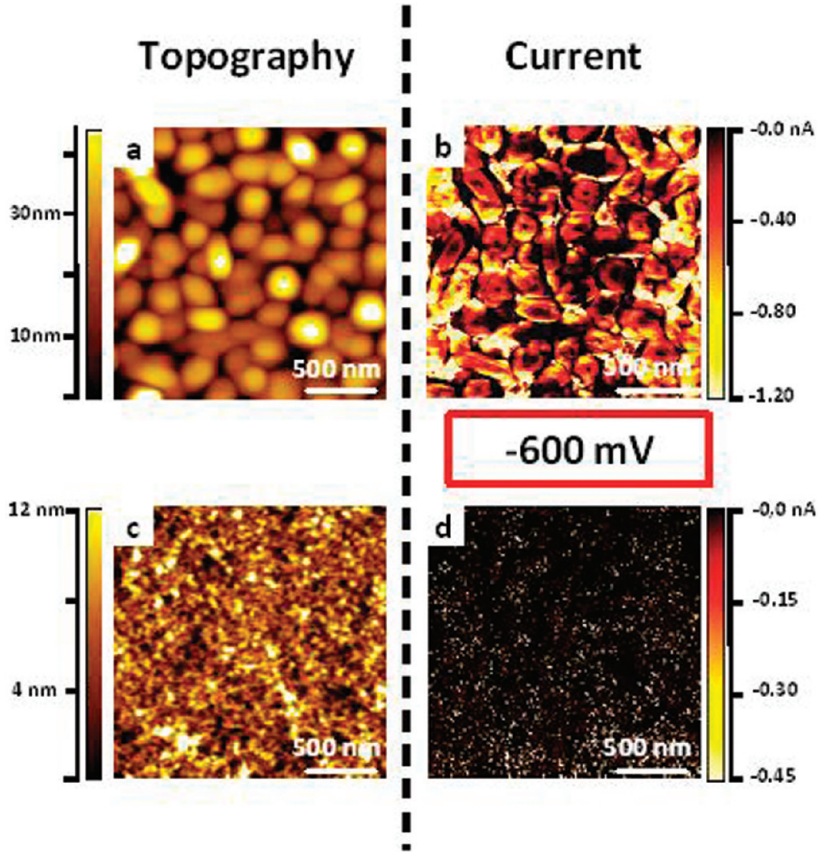

FIGURE 3. Contact-mode AFM topography image ($2 \times 2\ \mu m^2$) of (a) a DITPY-Ph_4 IFL and (c) a PEDOT:PSS IFL. CS-AFM current images recorded at −600 mV of the corresponding (b) DITPY-Ph_4 IFL and (d) PEDOT:PSS IFL deposited on ITO. Marked differences in the surface coverage, homogeneity, and intensity of the hole-carrying pathways are clearly observed between images b and d.

Comparison of the Electrical Channels of DITPY-Ph_4 and PEDOT:PSS IFL. The topography of a PEDOT:PSS IFL is shown in Figure 3c. The surface is highly uniform and smooth. The rms roughness is measured at 0.9 nm. This value is more than 6 times lower than that of the DITPY-Ph_4 IFL (rms = 5.5 nm). According to their morphologies, the PEDOT:PSS IFL should induce a better BHJ post-deposition compared to a DITPY-Ph_4 IFL. However, in sharp contrast to DITPY-Ph_4, the current image of the PEDOT:PSS IFL is almost entirely dark (Figure 3d). Most of the layer is thus composed of strong insulating regions. Besides, the hole-carrying pathways are very few and localized, approaching the resolution limit of the AFM technique. They correspond to individual PEDOT domains (15, 16, 19, 36). Finally, this current image reveals the detrimental microstructure inhomogeneities of PEDOT:PSS IFLs inherent to their polymeric networks. One key result is evidenced by an average threshold of both current images for current intensities down to 0.2 nA. Indeed, the total number of hole-carrying pathways is increased by more than 360% from a PEDOT:PSS IFL to a DITPY-Ph_4 IFL.

This considerable enhancement is of utmost importance in the decrease of both the series resistances and the rate of free hole recombination at trap sites into realistic OPV devices. These results thus constitute an additional argument in view of using DITPY-Ph_4 IFL to improve hole collection in OSCs.

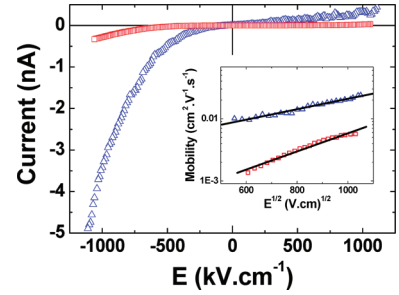

FIGURE 4. CS-AFM average local $I-E$ curves performed on an as-cast P3HT thin film (red squares) and a DITPY-Ph_4 single IFL (blue triangles). Inset: Extracted hole mobility according to a SCLC model, across as-cast P3HT (red squares) and DITPY-Ph_4 thin films (blue triangles).

3.1.2. Local Hole-Transport Properties in a DITPY-Ph_4 IFL. In order to check whether DITPY-Ph_4 IFLs can act as efficient hole-transport layers (HTLs), we performed single-point spectroscopy measurements by means of CS-AFM measurements. The local hole mobility of the organic thin film can then be quantified. As-cast and annealed P3HT thin films deposited on ITO are used as reference materials.

Qualitative Study: Space-Charge-Limited-Current (SCLC) Model. The same asymmetric behavior is observed on DITPY-Ph_4 and P3HT thin films (Figure 4). The current reaches its maximum under reverse bias and becomes very low when the tip is biased positively to the substrate. It is mainly attributed to the absence of an

injection barrier from the tip into the organics. A square dependence of the current under negative fields is measured on both of these two characteristics. The power law is typical of a SCLC (37−39). According to this regime, the charge transport follows the Mott−Gurney law defined as

$$J = 9/8\varepsilon_r\varepsilon_0\mu V^2/L^3 \quad (1)$$

where L is the thickness of the film, ε_r the dielectric constant of the organic material, ε_0 the vacuum permittivity, J the current density, V the tip bias, and μ the charge-carrier mobility.

Quantitative Study: Hole Mobility and Resistivity in DITPY-Ph$_4$ Thin Films. DITPY-Ph$_4$ and as-cast P3HT samples display large differences in their current intensities at negative fields (Figure 4). This is attributed to the higher hole mobility of the DITPY-Ph$_4$ thin film compared to the P3HT one. Because these single-point $I-E$ measurements fit with a SCLC model, the mobility values can be extracted using the Poole−Frenkel electric-field dependence, defined as

$$\mu = \mu_0 e(E/E_0)^{1/2} \quad (2)$$

where E is the electric field and equals V/L, μ_0 is the zero-field mobility, and E_0 is the field coefficient. As-cast P3HT films have a zero-field hole mobility of 2.0×10^{-4} $cm^2 \cdot V^{-1} \cdot s^{-1}$ (inset of Figure 4), which is consistent with recent CS-AFM measurements (38, 39). DITPY-Ph$_4$ IFL exhibits a mobility of 3.5×10^{-3} $cm^2 \cdot V^{-1} \cdot s^{-1}$, which is more than 1 order of magnitude higher than that of the as-cast P3HT film and equivalent to that of annealed P3HT (3.1×10^{-3} $cm^2 \cdot V^{-1} \cdot s^{-1}$). Because the current densities measured by CS-AFM are orders of magnitude higher than that obtained on typical planar hole-only devices, all of these hole mobility values are overestimated by the same amount. However, their relative comparison is of first relevance. Therefore, the hole mobility of DITPY-Ph$_4$ IFL is high enough to allow effective HTL properties and to ensure the collection of photogenerated charges in both as-cast and annealed (P3HT:PCBM) BHJ solar cells.

On the whole, these CS-AFM measurements reveal impressive advantages to using DITPY-Ph$_4$ thin films as IFLs between ITO and P3HT:PCBM BHJs. Cumulating intense and numerous hole-carrying pathways, having a high hole mobility, and ensuring a hole ohmic contact with ITO, DITPY-Ph$_4$ thin films overcome a lot of crucial limitations inherent to PEDOT:PSS IFLs and ITO/BHJ interfaces. We now demonstrate the hole collection efficiency of DITPY-Ph$_4$ thin films in OSCs, as both an independent HTL/EBL IFL and once associated with PEDOT:PSS as part of a double IFL.

3.2. Solar Cells Using a Single DITPY-Ph$_4$ IFL. We present here the OPV metrics of solar cells having the architecture {ITO/DITPY-Ph$_4$/P3HT:PCBM/LiF/Al}. At first, we have optimized their performances by varying both the thicknesses and the roughnesses of DITPY-Ph$_4$ IFLs. The most efficient {ITO/DITPY-Ph$_4$/P3HT:PCBM/LiF/Al} device is then compared to diodes having no IFL (direct postdeposition of the active layer on ITO) and to devices incorporating a 20-nm-thick layer of PEDOT:PSS. In this part of the study, none of the active layers were annealed.

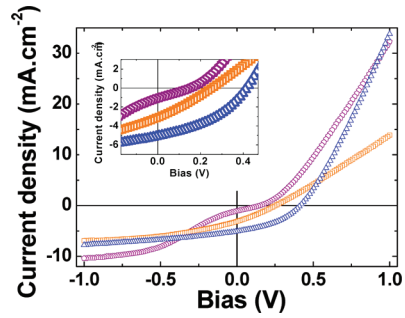

FIGURE 5. J_L-V characteristics measured on as-cast solar cells having the structures {ITO/DITPY-Ph$_4$(15 nm thickness and rms = 5.5 nm)/BHJ/LiF/Al} (blue triangles), {ITO/DITPY-Ph$_4$ (45 nm thickness and rms = 12.5 nm)/BHJ/LiF/Al} (orange squares), and {ITO/DITPY-Ph$_4$ (37 nm thickness and rms = 18.7 nm)/BHJ/LiF/Al} (purple pentagons), denoted as D2, D2b, and D2c, respectively.

3.2.1. Thickness and Roughness Effects of the DITPY-Ph$_4$ IFLs. We determine here the influence of both the thickness and the roughness of DITPY-Ph$_4$ IFLs on the OSC characteristics. For this, we compare three kinds of devices, {ITO/DITPY-Ph$_4$ (15 nm thickness and rms = 5.5 nm)/BHJ/LiF/Al}, {ITO/DITPY-Ph$_4$ (45 nm thickness and rms = 12.5 nm)/BHJ/LiF/Al}, and {ITO/DITPY-Ph$_4$ (37 nm thickness and rms = 18.7 nm)/BHJ/LiF/Al}, denoted as **D1**, **D1b**, and **D1c**, respectively. Their J_L-V curves are presented in Figure 5.

A noteworthy result is evidenced by comparing the OPV metrics of devices **D1b** and **D1c**, which mainly differ by the roughness of their DITPY-Ph$_4$ IFLs. Indeed, the performance of **D1c** ($V_{oc} = 0.15$ V; $J_{sc} = 1.02$ mA $\cdot$ cm^{-2}) is strongly lower than that of **D1b** ($V_{oc} = 0.25$ V; $J_{sc} = 3.04$ mA $\cdot$ cm^{-2}). As a consequence, the roughness of the DITPY-Ph$_4$ IFL is hardly detrimental on the OSC parameters. Concerning the decrease of J_{sc} in **D1c**, the effect of the roughness is intuitive, being easily understood by an increase in the shunts. However, the decrease in V_{oc} is impressive and highlights the fact that the roughness of the IFL can act to reduce this value, which is theoretically fixed by the donor HOMO and acceptor LUMO energy levels (2) in the case of electrical ohmic contacts. This comparison between the devices **D1b** and **D1c** (respectively 12.5 and 18.7 nm of DITPY-Ph$_4$) also reveals that the influence of the IFL is stronger than its thickness. Finally, a DITPY-Ph$_4$ IFL (15 nm thickness and rms = 5.5 nm) was designed to be thin enough in order to minimize both the light absorption and unproductive roughness of the surface, while maintaining a sufficient thickness for effective hole transport as well as electron-blocking properties. The performance of the device **D1** confirms the observations mentioned above, and its global efficiency is the highest that we have achieved by means of such architectures.

3.2.2. 15-nm-Thick Single DITPY-Ph$_4$ IFLs. Device **D1**, which possesses a 15-nm-thick DITPY-Ph$_4$ IFL, is

Table 1. PV Parameters (75 mW·cm^{-2}) of Devices with Different IFLs and (P3HT:PCBM) Active Layer Treatments: D1, D2, D3, and D4 Are As-Cast Active Layers and D5, D6, D7, and D8 Are Annealed Active Layers[a]

anodic interface	roughness (nm)	device	V_{oc} (V)	J_{sc} (mA · cm^{-2})	PCE (%)	α
ITO/DITPY-Ph$_4$	5.5	**D1**	0.42 (0.08)	5.1 (0.2)	1.11 (0.03)	0.86
		D5	0.49 (0.08)	7.7 (0.12)	2.02 (0.09)	0.87
Bare ITO	1.1	**D2**	0.51 (0.001)	4.0 (0.08)	1.02 (0.01)	0.77
		D6	0.58 (0.03)	7.0 (0.05)	1.73 (0.06)	0.84
ITO/PEDOT:PSS	0.9	**D3**	0.59 (0.003)	4.1 (0.21)	1.24 (0.01)	0.78
		D7	0.57 (0.02)	8.2 (0.15)	2.36 (0.17)	0.86
ITO/[DITPY-Ph$_4$/PEDOT:PSS]	3.2	**D4**	0.53 (0.15)	5.2 (0.07)	1.54 (0.08)	0.88
		D8	0.60 (0.03)	8.9 (0.14)	2.9 (0.02)	0.93

[a] The standard deviations of the average response parameters are indicated in parentheses.

here compared to reference solar cells having either no IFL or a 20-nm-thick PEDOT:PSS IFL. All measurements are performed under ambient atmosphere. The highest performances are obtained by using the polymeric IFL (V_{oc} = 0,66 V; J_{sc} = 4.7 mA · cm^{-2}). Meanwhile, the J_L−V plots emphasize the strong enhancement in J_{sc} of the device **D1** incorporating a 15-nm-thick DITPY-Ph$_4$ IFL. J_{sc} values of **D1** are about 25% and 10% higher than those in both of the two control diodes. However, V_{oc} of **D1** is lower by 90 and 240 mV compared to devices having no IFL or a PEDOT:PSS one (see Table 1).

The J_L−V characteristic of **D1** exhibits a well-designed concave shape in the fourth quadrant, thus confirming that the energy levels of DITPY-Ph$_4$ IFLs match those of P3HT and ITO and create a productive diode for hole extraction (8, 12, 40, 41). Whichever the IFL, the fill factors (FF) are in the range 37−40%, which is slightly below the theoretical 42% attainable by unbalanced hole/electron-transporting materials such as as-cast P3HT:PCBM BHJs (27−29). Furthermore, the DITPY-Ph$_4$ IFL effectively minimizes the series resistances and leads to the highest FF value (40%).

In order to explain the J_{sc} exaltation of **D1**, we performed profilometry and tapping-mode AFM experiments on the active layers of the three cells. Because similar thicknesses (110 ± 3 nm) are measured on every P3HT:PCBM film, the increase of J_{sc} in **D1** cannot be attributed to a higher number of absorbed photons. This enhancement of **D1** is attributed to a reduction of space-charge effects (27, 28) promoted by the strong hole sensitivity of DITPY-Ph$_4$ IFLs and by its HOMO energy level coincidence with that of P3HT. The EBL properties of the IFL, mediated by the LUMO energy level, contribute to blocking of the misdirected electrons at the anode and reduction of the rate of hole recombinations (29, 42). We will gain further investigation on these two physical processes below.

Concerning the decrease in V_{oc} of the device **D1**, three major causes can be responsible for it. A first possibility consists of having local p/n junctions between the DITPY-Ph$_4$ film and the PCBM grains. However, the action spectrum of the solar cell highlights the fact that the photocurrent generation remains restricted to the P3HT:PCBM active layer. Second, in the case of a nonohmic contact between the IFL and the active layer, V_{oc} is known to be lowered by the difference between the work functions of the anode and those of the cathode (2). However, this is not specific to any of the three devices because we find for each $V_{oc} \gg \Delta\phi_f = \phi_f(\text{ITO}) - \phi_f(\text{Al}) = 4.5 - 4.2 = 0.3$ V. Supplementary convincing evidence is brought out by CS-AFM measurements, which reveal that the contact of ITO with either P3HT or DITPY-Ph$_4$ is suitably ohmic. Besides, the aforementionned observations based on the FF and J_{sc} values of **D1** also confirm that the DITPY-Ph$_4$ IFL does not provide a counterproductive diode for hole extraction. Because we know that DITPY-Ph$_4$ IFLs provide adapted energy levels for the HOMO and the positive-integer charge transfer, one way to explain the lower V_{oc} values of **D1** is based on the roughness. Such an effect is known to play a major role (8, 21, 43). A prominent example is also established on our DITPY-Ph$_4$ IFLs. The DITPY-Ph$_4$ roughness impacts the chemical composition of the blended active layer and degrades its EBL/HTL properties.

3.3. Solar Cells Using a Double [DITPY-Ph$_4$/PEDOT:PSS] IFL. In order to smooth the DITPY-Ph$_4$ IFL responsible for unproductive effects on V_{oc}, a 5-nm-thick film of PEDOT:PSS was deposited on top. The surface of the *double IFL* is made of small PEDOT:PSS aggregates, having a fibrillar shape, and the roughness of the DITPY-Ph$_4$ IFL is decreased from 5.5 to 3.2 nm after its coating (Figure 2c).

While thicker films of PEDOT:PSS could easily reduce the residual roughness, the thickness is adjusted at 5 nm to retain the electronic and energetic properties of DITPY-Ph$_4$. It minimizes the probability for holes to recombine in the trapping sites inherent to PEDOT:PSS before reaching the efficient DITPY-Ph$_4$ hole-carrying pathways. Besides, for such low thicknesses, the PEDOT:PSS energetic contribution should be weak.

We investigate now devices having the architecture {ITO/[DITPY-Ph$_4$ (15 nm)/PEDOT:PSS (5 nm)]/P3HT:PCBM/LiF/Al}, denoted as **D4** for as-cast active layers and **D8** for annealed active layers. Such an architecture is compared to diodes having no IFL (**D2** when as-cast and **D6** when annealed) or incorporating either 15- or 5-nm-thick IFLs made of DITPY-Ph$_4$ (**D1** and **D5**) or PEDOT:PSS (**D3** and **D7**), respectively. The J_L−V parameters measured on the four devices under ambient atmosphere are summarized in Table 1. The question next arises as to whether P3HT:PCBM active

layers interact with the double IFL in the same way as they do with single IFLs of either DITPY-Ph_4 or PEDOT:PSS.

3.3.1. As-Cast P3HT:PCBM Films (D1, D2, D3, and D4). Adding a PEDOT:PSS IFL on top of DITPY-Ph_4 enhances the OPV performances of P3HT:PCBM solar cells (Table 1). Indeed, the device **D4** presents the highest PCE = 1.54% of the four as-cast diodes. Concerning V_{oc}, its value is measured at 0.53 V in **D4**. This is only slightly lower than that of device **D3** using a single PEDOT:PSS IFL, which is understood by means of the superior roughness of the double IFL. We can also notice that the J_{sc} is enhanced by more than 28% compared to the two control diodes **D2** and **D3**. We attribute this increase to the same physical causes that dictate the operation modes of devices having a single DITPY-Ph_4 IFL, which is the reduction of space-charge and recombination effects. These performances of the device **D4** confirm that the PEDOT:PSS top layer is thin enough to maintain the HTL/EBL properties of DITPY-Ph_4 and to decrease its roughness. By tuning the hole extraction efficiency of an ultrathin PEDOT:PSS IFL, the DITPY-Ph_4 layer leads to OPV metrics close to those previously obtained on a 20-nm-thick PEDOT:PSS device as well as the best results reported for as-cast P3HT:PCBM BHJs (8, 12, 21, 44, 45).

3.3.2. Annealed P3HT:PCBM Films (D5, D6, D7, and D8). Even though a higher PCE value (3.5%) is measured on a device using a 20-nm-thick PEDOT:PSS IFL, we essentially focus here on the operating mode induced by using DITPY-Ph_4. The OPV metrics of the control diode (V_{oc} = 0.64 V; J_{sc} = 8.60 V) are comparable to the best performances obtained at ambient atmosphere on this BHJ couple (8, 12, 21, 44, 45).

The annealing process of P3HT:PCBM thin films induces an overall improvement in the performance of each of the devices **D5** (a single DITPY-Ph_4 IFL), **D6** (no IFL), **D7** (PEDOT:PSS IFL), and **D8** (a double [DITPY-Ph_4/PEDOT:PSS] IFL). This is explained by a superior quality of the active layer, including a stronger phase segregation (1), decreases in the shunt resistances because of better-connected percolated networks (45), improved overlap with the solar spectrum (2), and balanced charge transport between holes and electrons (45). Figure 6 presents the J_L−V plots of the four annealed solar cells.

The device **D5** affords a PCE over 2%. The annealing temperature is not high enough to smooth the DITPY-Ph_4 surface; consequently, the roughness of the IFL still limits V_{oc}. Moreover, J_{sc} of **D5** (7.7 mA · cm^{-2}) is intermediate between those of **D6** (7.0 mA · cm^{-2}) and **D7** (8.6 mA · cm^{-2}). This means that the DITPY-Ph_4 IFL still allows a more efficient hole extraction than bare ITO. On the other hand, its interface with the annealed BHJ appears to be of poor quality, leading to the highest shunt resistances of the four annealed solar cells. Once more, the roughness of the DITPY-Ph_4 layer dramatically acts to reduce its substantial improvements caused by its strong HTL/EBL properties.

On the contrary, the device **D8** integrating the double [DITPY-Ph_4/PEDOT:PSS] IFL exhibits the highest global efficiency (PCE = 2.9%). Such a performance is achieved by

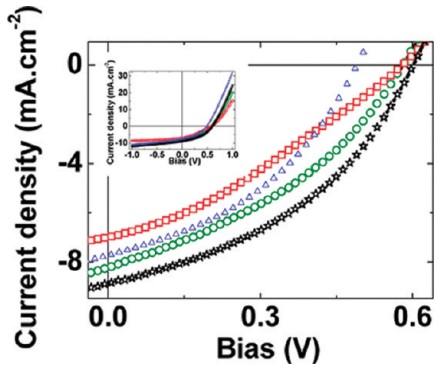

FIGURE 6. Focus in the fourth quadrant of the J_L−V characteristics corresponding to annealed solar cells. A comparison is made between devices having various IFLs: red squares when using no IFL, green circles when using PEDOT:PSS (5 nm), blue triangles when using DITPY-Ph_4(15 nm), and black stars when using a double [DITPY-Ph_4 (15 nm)/PEDOT:PSS (5 nm)] IFL.

means of better OPV metrics. At first, FF values of the two control diodes are lower because of misdirected electrons transferring from PCBM to ITO in **D7** and weak EBL properties in **D9**. Although **D8** is an annealed device, the highest FF value (41%) remains lower than expected. We propose that O_2 diffusion into the P3HT phase limits the improvement of the transport properties expected from the annealing process, thus decreasing the FF values. This hypothesis will be checked by the photocurrent-generation measurements below.

We also observed that the device **D8** possesses the highest V_{oc} value of the overall annealed solar cells (V_{oc} = 0.6 V). This result confirms that the DITPY-Ph_4 layer tunes the HTL/EBL properties of the 5-nm-thick PEDOT:PSS layer. In addition, **D8** exhibits the highest J_{sc} value (8.9 mA · cm^{-2}), which is 30% and 8% higher than solar cells using either no IFL or a single PEDOT:PSS IFL, respectively. Finally, this type of double HTL/EBL hole-collecting layer leads to a strong increase of about 65% and 25% in PCE compared to both types of reference diodes. This validates the design and implementation of a double [DITPY-Ph_4/PEDOT:PSS] IFL for high-performance P3HT:PCBM BHJ solar cells.

3.4. Photocurrent Generation. In order to gain further information on the solar cell operation modes and especially on the influence of DITPY-Ph_4 buffering, we have investigated dependences of the photocurrent density J_{ph} with the electric field and light intensity. J_{ph} is obtained by the difference $J_{ph} = J_L - J_D$, where J_L and J_D are the current densities under illumination and in the dark, respectively. The effective applied voltage (V_{eff}) is defined as $V_{eff} = V_0 - V$, with V being the applied voltage and V_0 the compensation voltage defined at $J_{ph} = 0$.

3.4.1. Photocurrent Generation in As-Cast P3HT:PCBM Solar Cells (D1, D2, D3, and D4). Field Dependence of the Photocurrent (J_{ph}). The photocurrent density of each of the four devices **D1** (a single DITPY-Ph_4 IFL), **D2** (no IFL), **D3** (PEDOT:PSS IFL), and **D4** ([DITPY-Ph_4/PEDOT:PSS] IFL) follows the same global increase with V_{eff} (Figure 7). This tendency corresponds to three types of regimes responsible for the photocurrent generation. In a first step, J_{ph} rises linearly with V_{eff}, as

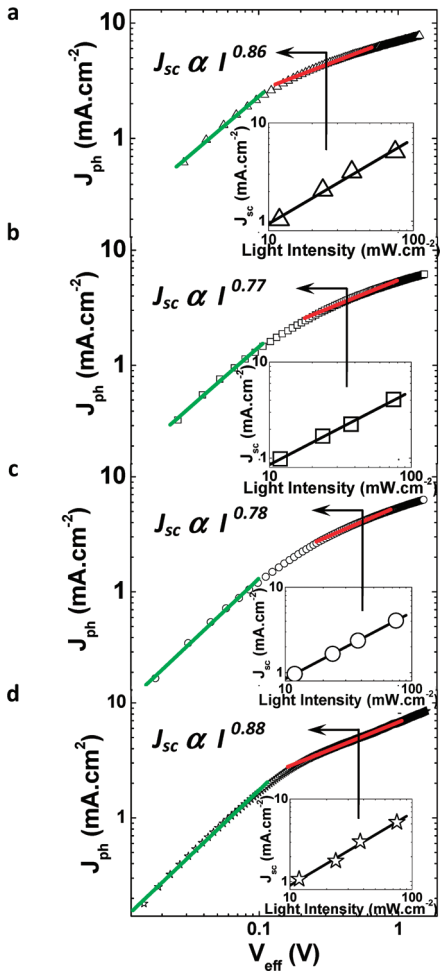

FIGURE 7. Photocurrent density J_{ph} as a function of the effective applied bias V_{eff} for as-cast P3HT:PCBM solar cells. The nature of the IFL is changed in each graph: (a) a single DITPY-Ph$_4$ (15 nm) IFL; (b) no IFL; (c) a single PEDOT:PSS (5 nm) IFL; (d) a double [DITPY-Ph$_4$ (15 nm)/PEDOT:PSS (5 nm)] IFL. The green line fits the linear behavior occurring at low applied bias, and the red line fits the square-root dependence of J_{ph}. The light-intensity dependence of J_{sc} is shown in the insets. Arrows indicate the scaling factor J_{sc} to the light intensity.

confirmed by the fitting lines in green. This is attributed to the strong competition between drift and diffusion currents happening for low electric fields (V_{eff} < 0.1 V). For a high reverse bias (V_{eff} > 1 V), J_{ph} gradually saturates (in our studies, V_{eff} is too low for the observation of a strong saturation of the photocurrent). Under these conditions, the photocurrent is field-independent and every photogenerated bound electron−hole pair is dissociated into free charge carriers (42).

The most relevant feature is observed on the square-root dependence (underlined by the fitting lines in red) for V_{eff} values (1 V > V_{eff} > 0.3 V). Because the dependence of J_{ph} with V_{eff} is square-root and not linear, monomolecular recombinations of geminate excitons do not constitute the major electrical loss mechanism. Once having ruled out this possibility, this means that none of the various IFLs completely suppress hole recombination processes. In the literature, this field-effect behavior is generally attributed to two fundamental contributions, being either the buildup of a space charge at the anode or effective bimolecular recombinations of free electron/hole carriers (42, 43). Unexpectedly, we note that the $J_{ph}-V_{eff}$ curves of the control diodes **D2** and **D5** are very close to each other. As a consequence, the internal electric field modified by the band bending created by accumulation of the charge carriers at the anode is not strongly influenced by the insertion of PEDOT:PSS. This can be explained by the ohmic contacts taking place at the anode. Similarly, the characteristics measured on devices using DITPY-Ph$_4$ IFLs do not reveal significant discrepancies, thus confirming the effective hole transfer from the active material to the external circuit. Meanwhile, this similarity prevents one from distinguishing the influence of each IFL on the electrical loss mechanisms occurring in the solar cells.

Light-Intensity Dependence of J_{sc}. Light-intensity (I_{Light}) measurements are performed on the four devices **D1**, **D2**, **D3**, and **D4**. J_{sc} gives direct insight of the photocurrent generation for 0.3 V < V_{eff} < 1 V. The insets in Figure 7 obviously demonstrate that the short-circuit currents follow a power law defined as $J_{sc} = I^{\alpha}_{Light}$. The scaling exponents α differ from device to device, as mentioned by the vertical arrows. The two control diodes **D2** (α = 0.77) and **D3** (α = 0.78) exhibit very similar values, which are likely equal to 0.75, being the archetypal value measured for space-charge-limited photocurrents (27−29, 42, 43). Therefore, J_{sc} is mainly limited in **D2** and **D3** by the buildup of free holes and by their extraction rate at the anode, in agreement with recent works (28, 45). The use of a 20-nm-thick PEDOT:PSS IFL does not bring an additional reduction of the hole accumulation region caused by this heavily unbalanced hole/electron charge transport into the active material (α = 0.79).

One key result of our study is that the two solar cells **D1** and **D4** possess the highest scaling exponents and equal 0.86 (for a single DITPY-Ph$_4$ IFL) and 0.88 (for a double [DITPY-Ph$_4$/PEDOT:PSS] IFL), respectively. These values are intermediate between that of a space-charge-limited (α = 0.75) and a monomolecular recombination-limited (α = 1) current. This means that a major part of the detrimental buildup made of free holes is reduced by the insertion of DITPY-Ph$_4$ at the anode. This improved hole collection underlines the strong HTL/EBL properties of every DITPY-Ph$_4$-based IFL and explains the exaltation of J_{sc} in as-cast P3HT-PCBM solar cells having both single and double DITPY-Ph$_4$-based IFLs.

3.4.2. Photocurrent Generation in Annealed P3HT:PCBM Solar Cells (D5, D6, D7, and D8). The scaling exponents measured on the two control diodes **D6** and **D7** are respectively equal to 0.84 and 0.86 and are also similar to that obtained when a 20-nm-thick PEDOT:PSS is used (α = 0.84). These values are higher than those obtained on equivalent as-cast devices. This is explained by the annealing procedure, which acts to establish a balanced charge transport between electrons and holes in the PCBM and P3HT phases (28). Indeed, percolated charge pathways are well-designed, and the buildup of free holes is reduced. We also note that these coefficients are slightly lower than the ones reported in the literature (45). This supports the effect of O_2 exposure, which still acts to reduce the enhanced

transport properties of the active material brought by the annealing process.

Interestingly, the values are very close to those measured lately on the aforementionned devices **D1** and **D4**. This means that the photocurrent generation in either as-cast or annealed P3HT:PCBM devices, having DITPY-Ph_4-based or reference IFLs, respectively, is not fully dictated by space-charge effects. To our knowledge, this unexpected partial transition regime from a space-charge-limited current to a recombination-limited current has never been achieved by insertion of a hole-collecting IFL.

We also notice that the device **D5** possesses a scaling factor α equal to 0.87. As a result, there is no change in the photocurrent generation regime between as-cast ($\alpha = 0.86$) and annealed devices having a single DITPY-Ph_4 IFL. On the contrary, α is equal to 0.93 for the annealed device **D9**. This value first demonstrates that residual space-charge effects can be suppressed by insertion of a double [DITPY-Ph_4/PEDOT:PSS] IFL. It also confirms that the interface quality between the DITPY-Ph_4-based IFLs and the P3HT:PCBM BHJ is an essential parameter in the efficiency of the hole extraction at the anode, as was previously described on the OPV metrics. Finally, all of these photocurrent generation studies confirm the drastic reduction of hole recombination rates brought by the strong HTL/EBL properties of semiconducting DITPY-Ph_4 films and validate their use as efficient HTL/EBL hole-collecting IFLs in P3HT:PCBM solar cells.

4. CONCLUSION

We have demonstrated that DITPY-Ph_4, a quinoid heterocyclic compound, behaves as an efficient IFL for hole collection in OSCs. We provide a detailed analysis of the characteristics of OSCs based on P3HT:PCBM BHJs fabricated without IFL, with either single PEDOT:PSS or single DITPY-Ph_4 IFLs, and with a double [DITPY-Ph_4/PEDOT:PSS (5 nm)] IFL. Nonannealed OSCs using a single DITPY-Ph_4 IFL exhibit a strong enhancement in J_{sc} of respectively 9% and ~23% compared to devices with an optimized 20-nm-thick PEDOT:PSS or without any IFL. CS-AFM also reveals a drastic increase of the hole-carrying pathways in DITPY-Ph_4 compared to those of PEDOT:PSS. In addition, a transition regime from space-charge-limited to recombination-limited photocurrents is evidenced between standard solar cells and those using a single DITPY-Ph_4 IFL. The role of DITPY-Ph_4 thin films is prominent in the hole extraction of the BHJs, and 15-nm-thick films are sufficient to create a more symmetric extraction of holes and electrons, as confirmed by equivalent annealed systems. Finally, covering the DITPY-Ph_4 IFL by an ultrathin film of PEDOT:PSS decreases its roughness and substantially increases the V_{oc} values of the solar cells. This top layer also reinforces the strong HTL/EBL properties of the single DITPY-Ph_4 IFL. These IFLs lead to recombination-limited devices having ~3% PCE under ambient conditions.

CS-AFM experiments allow nanoscale investigations of the physical operation modes of DITPY-Ph_4 IFLs. DITPY-Ph_4 thin films ensure a hole ohmic contact with ITO. They also develop a highly extended network made of intense current-carrying pathways compared to PEDOT:PSS, which drastically decreases series resistances and hole recombination at trapping sites in OSCs. In addition, the out-of-plane hole mobility of DITPY-Ph_4 IFLs is high enough to afford an efficient hole transport and collection.

Finally, single DITPY-Ph_4 and double [DITPY-Ph_4/PEDOT:PSS (5 nm)] HTL/EBL IFLs are applicable to almost the entire range of OSC devices. Using DITPY-Ph_4 IFLs can also improve the charge-injection efficiency in OLEDs. We are presently designing novel DITPY derivatives with the aim of tuning the electronic profile at the anodic interface of OSC devices.

Supporting Information Available: Syntheses, UV photoemission spectroscopy measurements, Figure S1, and references. This material is available free of charge via the Internet at http://pubs.acs.org.

REFERENCES AND NOTES

(1) Gaudiana, R.; Brabec, C. *Nat. Photonics* **2008**, *2*, 287–289.
(2) Dennler, G.; Scharber, M.; Ameri, T.; Denk, P.; Forberich, K.; Waldauf, C.; Brabec, C. *Adv. Mater.* **2008**, *20*, 579–583.
(3) Liang, Y.; Xu, Z.; Xia, J.; Tsai, S.-T.; Wu, Y.; Li, G.; Ray, C.; Yu, L. *Adv. Mater.* **2010**, *22*, E135—E138.
(4) Park, S. H.; Roy, A.; Beaupré, S.; Cho, S.; Coates, N.; Moon, J. S.; Moses, D.; Leclerc, M.; Lee, K.; Heeger, A. *Nat. Photonics* **2009**, *3*, 297–302.
(5) Uhrich, C.; Schueppel, R.; Petrich, A.; Pfeiffer, M.; Leo, K.; Brier, E.; Kilickiran, P.; Baeuerle, P. *Adv. Funct. Mater.* **2007**, *17*, 2991–2999.
(6) Campoy-Quiles, M.; Ferenczi, M.; Agostinelli, T.; Etchegoin, T.; Kim, P. G.; Anthopoulos, Y.; Stavrinou, T. D.; Bradley, P. N.; Nelson, D. D. C. *Nat. Mater.* **2008**, *7*, 158–164.
(7) Irwin, M. D.; Buchholz, D. B.; Hains, A. W.; Chang, R. P.; Marks, T. J. *Proc. Natl. Acad. Sci. U.S.A.* **2008**, *105*, 2783.
(8) Hains, A. W.; Ramanan, C.; Irwin, M. D.; Liu, J.; Wasielewski, M. R.; Marks, T. J. *ACS Appl. Mater. Interfaces* **2010**, *2*, 175–185.
(9) Ma, H.; Yip, H.; Huang, F.; Jen, A. K. *Adv. Funct. Mater.* **2010**, doi: 10.1002/adfm.200902236.
(10) Hains, A. W.; Liu, J.; Martinson, A. B. F.; Irwin, M. D.; Marks, T. J. *Adv. Funct. Mater.* **2010**, *20*, 595–606.
(11) Steim, R.; Kogler, F. R.; Brabec, C. J. *J. Mater. Chem.* **2010**, *20*, 2499.
(12) Wei, H.; Huang, J.; Ho, K.; Chu, C. *ACS Appl. Mater. Interfaces* **2010**, *2*, 1281–1285.
(13) Aleshin, A. N.; Williams, S. R.; Heeger, A. J. *Synth. Met.* **1998**, *94*, 173–177.
(14) Ouyang, J.; Chu, C. W.; Chen, F. C.; Xu, Q.; Yang, Y. *Adv. Funct. Mater.* **2005**, *15*, 203–208.
(15) Levermore, P.; Chen, L.; Wang, X.; Das, R.; Bradley, D. *Adv. Mater.* **2007**, *19*, 2379–2385.
(16) Kemerink, M.; Timpanaro, S.; de Kok, M. M.; Meulenkamp, E. A.; Touwslager, F. J. *J. Phys. Chem. B* **2004**, *108*, 18820–18825.
(17) Groenendaal, L.; Zotti, G.; Aubert, P. H.; Waybright, S. M.; Reynolds, J. R. *Adv. Mater.* **2003**, *15*, 855–879.
(18) Nardes, A.; Kemerink, M.; Janssen, R. A. J.; Bastiaansen, J.; Kiggen, N.; Langeveld, B.; van Breemen, A.; de Kok, M. *Adv. Mater.* **2007**, *19*, 1196–1200.
(19) Pingree, L. S. C.; MacLeod, B. A.; Ginger, D. S. *J. Phys. Chem. C* **2008**, *112*, 7922–7927.
(20) Hatton, R. A.; Willis, M. R.; Chesters, M. A.; Rutten, F. J.; Briggs, D. *J. Mater. Chem.* **2003**, *13*, 38–43.
(21) Kim, J. S.; Park, J. H.; Lee, J. H.; Jo, J.; Kim, D.; Cho, K. *Appl. Phys. Lett.* **2007**, *91*, 112111.
(22) Campbell, I. H.; Kress, J. D.; Martin, R. L.; Smith, D. L.; Barashkov, N. N.; Ferraris, J. P. *Appl. Phys. Lett.* **1997**, *71*, 3528.
(23) Armstrong, N. R.; Carter, C.; Donley, C.; Simmonds, A.; Lee, P.; Brumbach, M.; Kippelen, B.; Domercq, B.; Yoo, S. *Thin Solid Films* **2003**, *445*, 342–352.

(24) Khodabakhsh, S.; Poplavskyy, D.; Heutz, S.; Nelson, J.; Bradley, D. D.; Murata, H.; Jones, T. S. *Adv. Funct. Mater.* **2004**, *14*, 1205–1210.
(25) Heimel, G.; Romaner, L.; Zojer, E.; Bredas, J.-L. *Acc. Chem. Res.* **2008**, *41*, 721–729.
(26) Choulis, S.; Choong, V.; Patwardhan, A.; Mathai, M.; So, F. *Adv. Funct. Mater.* **2006**, *16*, 1075–1080.
(27) Mihailetchi, V.; Wildeman, J.; Blom, P. W. M. *Phys. Rev. Lett.* **2005**, *94*, 126602.
(28) Koster, L. J. A.; Mihailetchi, V. D.; Xie, H.; Blom, P. W. M. *Appl. Phys. Lett.* **2005**, *87*, 203502.
(29) Lenes, M.; Morana, M.; Brabec, C. J.; Blom, P. W. M. *Adv. Funct. Mater.* **2009**, *19*, 1106–1111.
(30) Casado, J.; Zgierski, M.; Delgado, M.; Navarrete, J.; Mas-Torrent, M.; Rovira, C. *J. Phys. Chem. C* **2007**, *111*, 10110–10118.
(31) Alves, H.; Molinari, A. S.; Xie, H.; Morpurgo, A. F. *Nat. Mater.* **2008**, *7*, 574–580.
(32) Berridge, R.; Skabara, P. J.; Pozo-Gonzalo, C.; Kanibolotsky, A.; Lohr, J.; McDouall, J. J. W.; McInnes, E. J. L.; Wolowska, J.; Winder, C.; Sariciftci, N. S.; Harrington, R. W.; Clegg, W. *J. Phys. Chem. B* **2006**, *110*, 3140–3152.
(33) Bolag, A.; Mamada, M.; Xie, H.; Nishida, J.-I.; Yamashita, Y. *Chem. Mater.* **2009**, *21*, 4350–4352.
(34) Gionis, V.; Fugnitto, R.; Meyer, G.; Strzelecka, H.; Dubois, J. C. *Mol. Cryst. Liq. Cryst.* **1982**, *90*, 153.
(35) Chasseau, D.; Gaultier, J.; Hauw, C.; Fugnitto, R.; Gionis, V.; Strzelecka, H. *Acta Crystallogr.* **1982**, *38*, 1629.
(36) Schaarschmidt, A.; Farah, A. A.; Aby, A.; Helmy, A. S. *J. Phys. Chem. B* **2009**, *113*, 9352–9355.
(37) Braun, S.; Salaneck, W. R.; Fahlman, M. *Adv. Mater.* **2009**, *21*, 1450–1472.
(38) Reid, O. G.; Munechika, K.; Ginger, D. S. *Nano Lett.* **2008**, *8*, 1602–1609.
(39) O'Douheiret, O.; Lutsen, L.; Swinnen, A.; Breselge, M.; Vandewal, K.; Goris, L.; Manca, J. *Appl. Phys. Lett.* **2006**, *89*, 032107.
(40) Bohnenbuck, B.; von Hauff, E.; Parisi, J.; Deibel, C.; Dyakonov, V. *J. Appl. Phys.* **2006**, *99*, 024506.
(41) Gupta, D.; Bag, M.; Narayan, K. S. *Appl. Phys. Lett.* **2008**, *92*, 093301.
(42) Mihailetchi, V.; Koster, L.; Hummelen, J.; Blom, P. W. M. *Phys. Rev. Lett.* **2004**, *93*, 216601–1.
(43) Moulé, A.; Meerholz, K. *Appl. Phys. B: Laser Opt.* **2008**, *92*, 209–218.
(44) Padinger, F.; Rittberger, R. S.; Sariciftci, N. S. *Adv. Funct. Mater.* **2003**, *13*, 85–88.
(45) Mihailetchi, V.; Xie, H.; de Boer, B.; Koster, L.; Blom, P. W. M. *Adv. Funct. Mater.* **2006**, *16*, 699–708.

AM1005546